International Journal of Biological Macromolecules 91 (2016) 578–588

Contents lists available at ScienceDirect

International Journal of Biological Macromolecules

journal homepage: www.elsevier.com/locate/ijbiomac

Doxorubicin-loaded fucoidan capped gold nanoparticles for drug delivery and photoacoustic imaging

Panchanathan Manivasagan[a], Subramaniyan Bharathiraja[a], Nhat Quang Bui[b], Bian Jang[a], Yun-Ok Oh[a], In Gweon Lim[c], Junghwan Oh[a,b,*]

[a] Marine-Integrated Bionics Research Center, Pukyong National University, Busan 608-737, Republic of Korea
[b] Department of Biomedical Engineering and Center for Marine-Integrated Biotechnology (BK21 Plus), Pukyong National University, Busan 608-737, Republic of Korea
[c] Department of Mechanical Engineering, Myong-Ji University, San 38-2, Nam-Dong, Cheoin-Gu, Yongin-Si, Gyeonggi-Do 449-728, Republic of Korea

ARTICLE INFO

Article history:
Received 19 April 2016
Received in revised form 11 May 2016
Accepted 2 June 2016
Available online 3 June 2016

Keywords:
Fucoidan
Gold nanoparticles
Doxorubicin
Drug delivery
Photoacoustic imaging

ABSTRACT

Polymer nanoparticles are emerging as a useful tool for a wide variety of biomedical and therapeutic applications. The present study demonstrates the multifunctional doxorubicin-loaded fucoidan capped gold nanoparticles (DOX-Fu AuNPs) for drug delivery and photoacoustic imaging (PAI). Biocompatible AuNPs were synthesized using a naturally occurring fucoidan (Fu) as a capping and reducing agent. The Fu AuNPs synthesis was determined using UV–visible spectrum, and it was further characterized using high resolution transmission electron microscopy, energy dispersive X-ray spectroscopy, Fourier transform infrared spectroscopy, and X-ray diffraction analysis. The release of DOX from DOX-Fu AuNPs was greater in acidic pH (4.5) than in neutral pH (7.4). The *in vitro* cytotoxic effect of fucoidan, Fu AuNPs, DOX, and DOX-Fu AuNPs inhibited the proliferation of human breast cancer cells with an inhibitory concentration of 35 μg/mL, 30 μg/mL, 15 μg/mL, and 5 μg/mL at 24 h. DOX-Fu AuNPs induced both early and late apoptosis in a concentration-dependent manner compared with untreated control cells. The ability of DOX-Fu AuNPs as a contrast agent for *in vitro* breast cancer imaging with PAI has been evaluated. These results suggest that the multifunctional DOX-Fu AuNPs for drug delivery and PAI can soon provide considerable contribution to human health.

1. Introduction

Polymer nanoparticles are considered excellent candidates as nanomedicine, with a high potential for diagnostic and therapeutic purposes with the possibility to achieve site-specific drug delivery because of its high degree of safety and other favorable properties such as biocompatibility, biodegradability, and nontoxic nature [1]. Marine polymers are interesting biomaterials, which can be used for obtaining biomimetic nanoparticles with tunable surface properties. There is growing interest in them considering the increasing number of researchers reporting the use of marine polymers as capping materials to design novel nanoparticles for imaging, delivery, and targeting in cancer therapy during the last few years [2]. Fucoidan is a naturally occurring sulfated polysaccharide extracted from marine brown seaweeds, containing large proportions of L-fucose and sulfate including *Fucus vesiculosus* [3]. Fucoidan was used as an immuno-therapeutic function polymer and is an excellent drug candidate for pharmaceutical applications [4]. It has a wide spectrum of activity in biological systems, including antibacterial, antiviral, antitumor, anti-inflammatory, anticoagulant, immunomodulatory and antithrombotic effects [5].

Metal nanoparticles are new generation nanomaterials with biomedical and therapeutic applications. Gold nanoparticles (AuNPs) owing to their desirable optical, electrical, and chemical properties have attracted a great deal of attention during recent decades [6–8]. The synthesis of AuNPs normally involves the reduction of positively charged gold atom and addition of stabilizing agents. The chemical used for gold synthesis is normally citrate, sodium borohydride, and organic compounds [9]. To reduce the use of chemical and toxic waste to the environment, the synthesis of AuNPs using natural compounds is of interest. Among them, fucoidan has been employed for the synthesis of AuNPs. To this end, interest in this field has increased utilizing biocompatible, biodegradable, and nontoxic naturally occurring marine polymers

* Corresponding author at: Marine-Integrated Bionics Research Center, Pukyong National University, Busan 608-737, Republic of Korea. Fax: +82 51 629 5779.
E-mail address: jungoh@pknu.ac.kr (J. Oh).

http://dx.doi.org/10.1016/j.ijbiomac.2016.06.007
0141-8130/

such as chitosan [10] and porphyran [11] for rapid synthesis of AuNPs and subsequent use for drug delivery applications.

Doxorubicin (DOX) is a widely used chemotherapeutic agent [12]. Although it kills the cancerous cells by inhibiting the synthesis of nucleic acids within cells, three main problems are encountered with DOX, first, high toxicity and large volume of distribution, second, short life time in the body and third low solubility which results in a narrow therapeutic index [13,14]. To overcome the non-specificity and high toxicity of DOX, many researchers have proposed conjugation to hydrophilic polymers to reduce the toxicity level while sustaining the therapeutic efficacy [14]. Fucoidan is biopolymer, which is completely water soluble, biocompatibility, biodegradable and nontoxic in nature.

Breast cancer is the second leading cause of cancer death among women in developed countries and is also increasingly observed in developing countries. In the United States alone, it is estimated that 39,620 breast cancer deaths and 232,340 new cases are expected among women in 2013 [15]. In the new millennium, the expected number of annual new cases of breast cancer worldwide could exceed 1.5 million [16]. The existing cytotoxic agents used for breast cancer treatment are expensive and inefficient because of severe side effects induced due to their toxicity in noncancerous tissues [17]. Therefore, it is of the utmost importance to develop new therapeutic agents that are biocompatible and cost-effective. In recent years, nanotechnology-based products, such as nano-drug, nano-cars, nano-dresses, skin creams, ball, and tennis rackets have been increasingly introduced into the global market. To date, as many as 1628 nano-based products are being extensively used for various purposes worldwide. Inorganic nanoparticles have already been utilized in wound healing and antibacterial applications [18].

Photoacoustic tomography (PAT) referred to as optoacoustic tomography is a hybrid, nonionizing imaging modality that combines the merits of both optical and ultrasonic imaging methods [19]. It is currently attracting immense interest in the biomedical optical imaging field. Photoacoustic imaging (PAI) is a new imaging modality under preclinical development that has been applied to various biomedical application for obtaining anatomic and functional information, including breast tumor detection, epidermal melanin measurements, blood oxygenation monitoring, and quantitative blood flow estimation [20–22]. Tissue-mimicking polyvinyl alcohol (PVA) phantom is an important tool for performance testing and optimization of medical ultrasound systems and photoacoustic devices as well as for medical training purposes. Hence, the ideal phantom material possesses acoustic and optic properties similar to those of human tissue. AuNPs have been used as contrast agents for imaging with PAT *in vitro* [23]. In the present study, a novel strategy was undertaken to exploit the use of fucoidan as a reducing agent for the green synthesis of AuNPs and subsequently loaded with DOX to demonstrate their use for drug delivery and PAI.

2. Materials and methods

2.1. Chemicals

Fucoidan from *Fucus vesiculosus* and Gold (III) chloride trihydrate ($HAuCl_4{\cdot}3H_2O$) was purchased from Sigma–Aldrich (St. Louis, USA). Doxorubicin hydrochloride (DOX) was obtained from Sigma–Aldrich (St. Louis, USA). A yellow tetrazole, 3-(4,5-dimethylthiazol-2-yl)-2,5-diphenyltetrazolium bromide (MTT) was purchased from Sigma–Aldrich (St. Louis, USA). All chemicals were of analytical grade and procured from Sigma–Aldrich (St. Louis, USA).

2.2. Synthesis of gold nanoparticles

Fucoidan was obtained using previously described methods [24–26]. Briefly, 0.005 g of fucoidan was added to 10 mL aqueous solution of 1×10^{-4} M $HAuCl_4{\cdot}3H_2O$, and the solution was kept in magnetic heater stirrer at 80 °C for 30 min, which resulted in a dark ruby red color indicating the formation of AuNPs. The formation of AuNPs was monitored with UV–visible spectroscopy using Beckman Coulter DU530 Life Science UV/vis spectrophotometer (Beckman Coulter, Fullerton, CA, USA). Synthesized AuNPs were collected by centrifugation at 12,000*g* for 30 min and washed many times with deionized water by centrifugation and re-dispersion in water to remove excess gold. The AuNPs dispersion was dialyzed using dialysis tube with a 12,000 Da molecular weight cutoff for 24 h to remove ionic impurities.

2.3. Preparation of doxorubicin-loaded fucoidan capped gold nanoparticles

A calculated amount of DOX was added to AuNPs dispersion, obtained as described above, resulting in a final DOX concentration of 10^{-4} M in solution. The mixture of DOX and AuNPs dispersion was incubated for 24 h at room temperature and then centrifuged at 10,000*g* for 15 min. The obtained pellet after centrifugation was separated from the supernatant solution and redispersed in deionized water prior to further characterization [11].

Drug loading was calculated using two methods: first method is based on the indirect method by estimating DOX content of the supernatant, and second is based on the direct method by estimating DOX content present in the pellet obtained after centrifugation. The drug concentration in supernatant and redispersed pellet were determined by measurements of its UV absorbance at 480 nm using UV–visible spectroscopy and the percentage loading of DOX on to AuNPs was estimated by the following formula:

$$\%\text{Drug loading efficiency} = \frac{\text{Total amount of DOX added} - \text{amount of DOX in supernatant or redispersed pellet}}{\text{Total amount of DOX added}} \times 100$$

2.4. Characterization of fucoidan capped gold nanoparticles and doxorubicin-loaded fucoidan capped gold nanoparticles

Studies on size, morphology, and composition of fucoidan capped gold nanoparticles (Fu AuNPs) and DOX-loaded fucoidan capped gold nanoparticles (DOX-Fu AuNPs) were performed using field emission scanning electron microscopy (FESEM; JSM-6700, JEOL, Japan), high resolution transmission electron microscopy (HRTEM; JEM 1010, JEOL, Japan), and energy dispersive X-ray spectroscopy (EDX). Fourier transform infrared spectroscopy (FTIR) spectra of fucoidan, Fu AuNPs, DOX, and DOX-Fu AuNPs were performed using spectrum GX spectrometry in diffuse reflectance mode operated at a resolution of 4 cm^{-1} of wavelength of approximately 4000–400 cm^{-1}. X-ray diffraction (XRD) analysis (X'Pert-MPD, Philips, Netherlands) was performed by preparing a thin film of powdered Fu AuNPs. The particle size analysis was determined by dynamic light scattering (DLS) method using electrophoretic light scattering spectrophotometer (ELS-8000, OTSUKA Electronics Co. Ltd., Japan) at a fixed angle of 90° and at room temperature. The zeta potential (ZP) of the AuNPs before and after loading DOX was measured with an electrophoretic light scattering spectrophotometer (ELS-8000, OTSUKA Electronics Co. Ltd., Japan) using ELS FlatBoard cell. The stability of Fu AuNPs was assessed at ambient temperature. The change in surface plasmon resonance

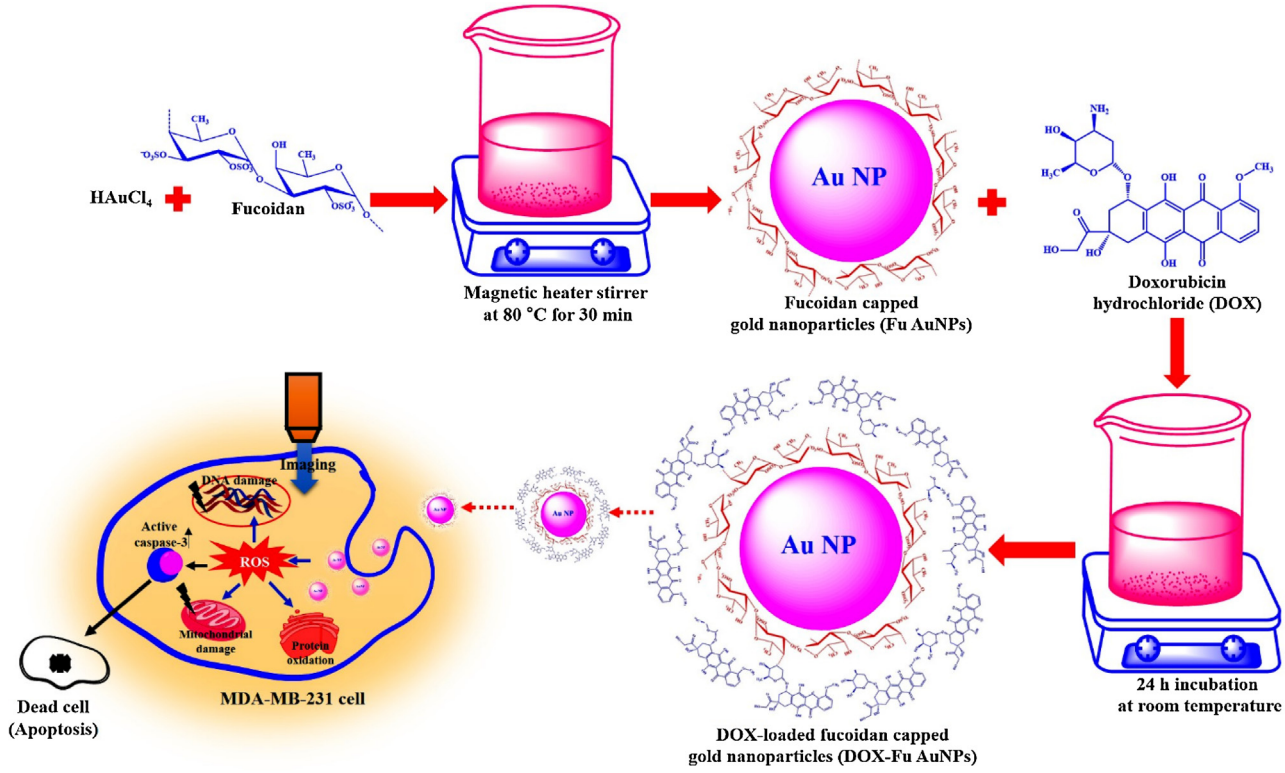

Scheme 1. Schematic diagram showing fucoidan capped gold nanoparticles and subsequent loading of doxorubicin on fucoidan capped gold nanoparticles for drug delivery and photoacoustic imaging.

(SPR) of nanoparticles dispersion was recorded up to 6 months using by UV–visible spectroscopy.

2.5. In vitro *drug release*

DOX-Fu AuNPs (1 mL) was dialyzed against 10 mL of phosphate buffered saline solution (PBS, pH 7.4) using a cellulose acetate membrane (spectra, MWCO: 1000 Da) in a magnetic heater stirrer at 37 °C with continuous stirring at 100 rpm. At the designated time interval, all outer solutions were exchanged from fresh PBS solution, and the solution containing released DOX was used for quantitative analysis. The amount of DOX released was analyzed using a spectrophotometer at 490 nm. A similar release study was conducted in acetate buffer (pH 4.5). The experiments were performed in triplicates for each sample.

2.6. In vitro *cytotoxic activity*

2.6.1. *Cell viability assay*

Human breast cancer cell line (MDA-MB-231) was purchased from Korean Cell Line Bank Seoul, South Korea and was grown in Dulbecco's Modified Eagle Medium (DMEM). Cells were seeded into 96-well plates at approximately 5×10^4 cells at 37 °C in a 5% CO_2 atmosphere. Cells were treated with different concentration of fucoidan, Fu AuNPs, DOX, and DOX-Fu AuNPs (5, 10, 15, 20, 25, 30, 35, 40, 45, and 50 μg/mL) for 24 h incubation [27]. Treated cells were incubated for 24 h to perform cytotoxic analysis using MTT assay. MTT was prepared at a concentration of 0.5 mg/mL and 100 μL of MTT was added in each well and incubated for 4 h. Purple formazone crystals were observed, and these crystals were dissolved with 100 μL of dimethyl sulfoxide (DMSO) and read at 570 nm using a multi-well ELISA plate reader [28]. Optical density value was subjected to the percentage of viability using the following formula:

$$\text{Percentage of cellviability}\,(\%) = \frac{\text{OD value of experimental samples}}{\text{OD value of experimental controls}} \times 100$$

2.6.2. *Morphological observation*

MDA-MB-231 cells were treated with different concentrations of DOX-Fu AuNPs and incubated for 24 and 48 h at 37 °C in a 5% CO_2 atmosphere. After the incubation of cells, gross morphological changes in the cell were observed under a Leica DMI3000 B inverted phase contrast microscope (Leica Microsystems GmbH, Wetzlar, Germany).

2.6.3. *Propidium iodide staining*

MDA-MB-231 cells were plated at 5×10^4 cells/well into a 6-well plate. At >90% confluence, cells were treated with DOX-Fu AuNPs for 24 and 48 h. Cells were washed with PBS and fixed in methanol: acetic acid (3:1 v/v) for 10 min. After fixation, they were stained with 50 μg/mL of propidium iodide (PI; Sigma–Aldrich, St. Louis, USA) for 20 min. Nuclear morphology of apoptotic cells with condensed/fragmented nuclei was examined under a fluorescence microscope (Leica Microsystems GmbH, Wetzlar, Germany).

2.6.4. *DAPI (4′,6-diamidino-2-phenylindole dihydrochloride) staining*

MDA-MB-231 cells were treated with DOX-Fu AuNPs for 24 and 48 h and then fixed with methanol:acetone (3:1, v/v) prior to washing with PBS. Washed cells were then stained using 1 mg/mL 4′,6-diamidino-2-phenylindole dihydrochloride (DAPI; Sigma–Aldrich, St. Louis, USA) for 30 min in the dark. Nuclear morphology was examined under a fluorescence microscope (Leica

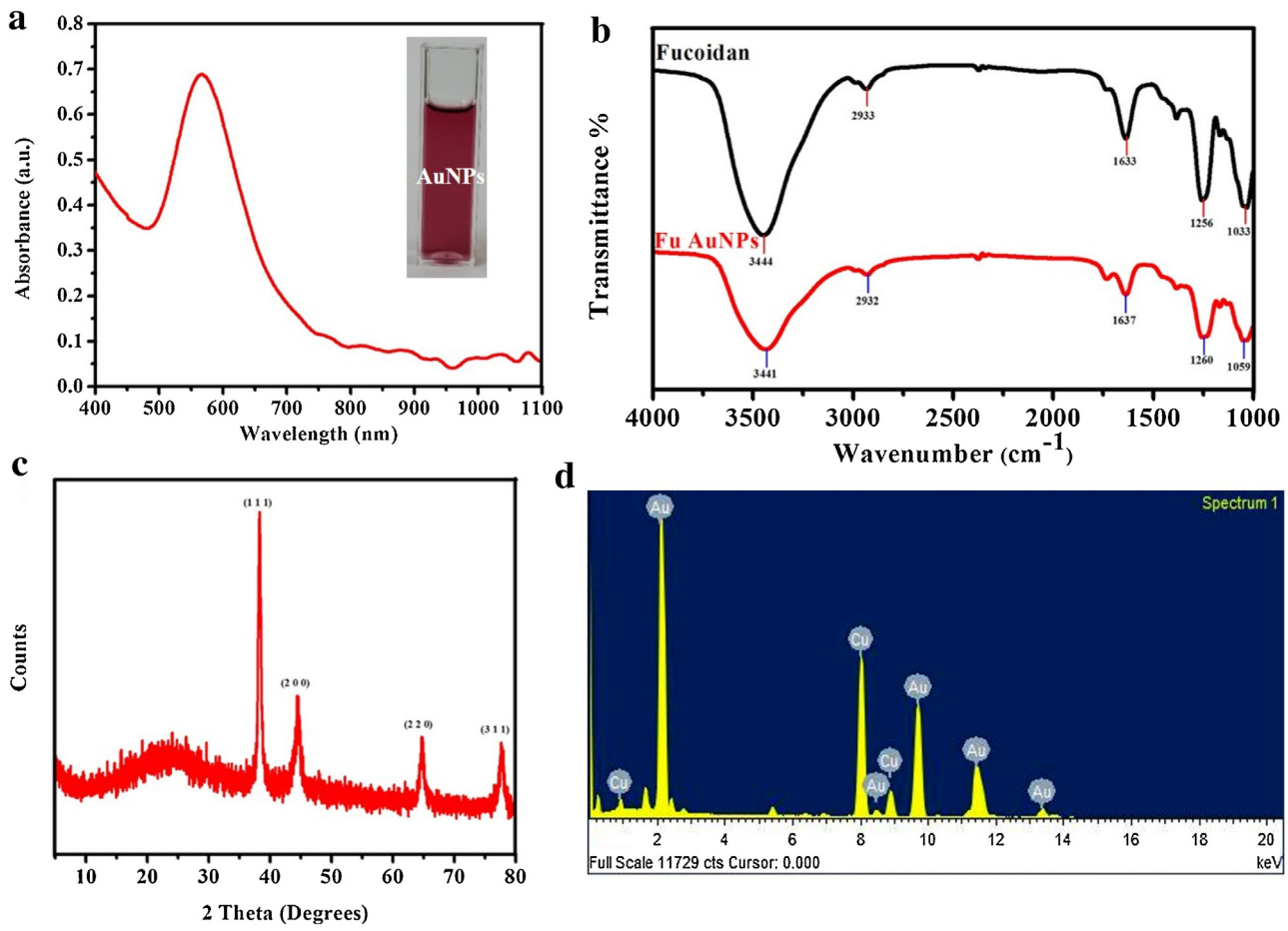

Fig. 1. (a) UV-vis spectral analysis of fucoidan capped gold nanoparticles. (b) FTIR spectra of fucoidan and fucoidan capped gold nanoparticles. (c) XRD pattern of fucoidan capped gold nanoparticles. (d) Energy dispersive X-ray spectrum of fucoidan capped gold nanoparticles.

Microsystems GmbH, Wetzlar, Germany) to identify cells undergoing apoptosis.

2.6.5. Cell cycle analysis by flow cytometry

MDA-MB-231 (5×10^4 cells/well) cells were seeded into 6-well culture plates and incubated for 24 and 48 h for cell attachment and recovery. Cells were treated with an inhibitory concentration (IC_{50}) of DOX-Fu AuNPs for 24 and 48 h. Untreated cells (control) were also incorporated. After incubation, cells were harvested and fixed with ice-cold 70% ethanol (5 mL) at −20 °C. They were allowed to stand overnight, and cell pellets were further processed using the FITC Annexin V Apoptosis Detection Kit (BD Pharmingen™) according to the manufacturer's protocol by fluorescent activated cell sorter (FACS) analysis (BD FACSVerse, NJ, USA) [29].

2.7. Photoacoustic tomography

The noninvasive PAI system has been previously developed and described [30]. In the present study, we modified the system to use only the pumping light (532 nm pump source, 10 Hz repetition rate, and 3–5 ns pulse width) from the Q-switched pulsed Nd:YAD laser (Surelite III, Continuum, CA, USA) (Fig. 7a). The free-space output laser beam was coupled with a 0.22-NA, 600-μm core diameter, multi-mode optical fiber (Thorlabs, NJ, USA) with a plano–convex lens of 50 mm in focal length (Thorlabs). The input end of the optical fiber was fixed to a fiber coupler at the focus point of the lens. The output end of the fiber was combined with a 10-MHz single element, focused transducer (Panametrics, MA, USA) and aligned such that the center of the irradiated light would locate at the focal point of the transducer. The output end of the fiber and transducer were mounted on a three dimensional linear actuator and moved for raster scanning. Output signals from the US transducer were amplified using an ultrasound pulser/receiver (5900 PR, Olympus, MA, USA). Then, the signals were digitized and stored using a data acquisition (DAQ) system which includes a 100-MS/s DAQ card (PXI-5122, National Instruments, TX, USA) and an embedded controller (PXI-1042Q, National Instruments). The trigger signals from the laser system were synchronized with the DAQ system to capture photoacoustic signals when the pulsed laser irradiated the sample. The DAQ system was controlled by a custom-made LabView program. To form photoacoustic image, acquired photoacoustic signals were post processed to improve image quality by applying bandpass filtered (3–20 MHz) to reduce noise. The Hilbert transform was used to detect the signal envelope by taking the absolute values of analytic signals. Finally, envelope signals were used to construct three dimensional photoacoustic image using a home-made Matlab program.

2.7.1. Doxorubicin-loaded fucoidan capped gold nanoparticles labeling of MDA-MB-231 cells

Cells (3×10^5 cells/well) were treated with two different concentrations of DOX-Fu AuNPs (5 and 10 μg/mL) and incubated for 24 h at 37 °C. Untreated cells (3×10^5 cells) were used as a control. After 24 h, cells were washed with 1 × PBS, and morphological changes in cells were observed under a Leica DMI3000 B inverted phase contrast microscope (Leica Microsystems GmbH, Wetzlar, Germany). Treated and untreated cells were harvested and fixed

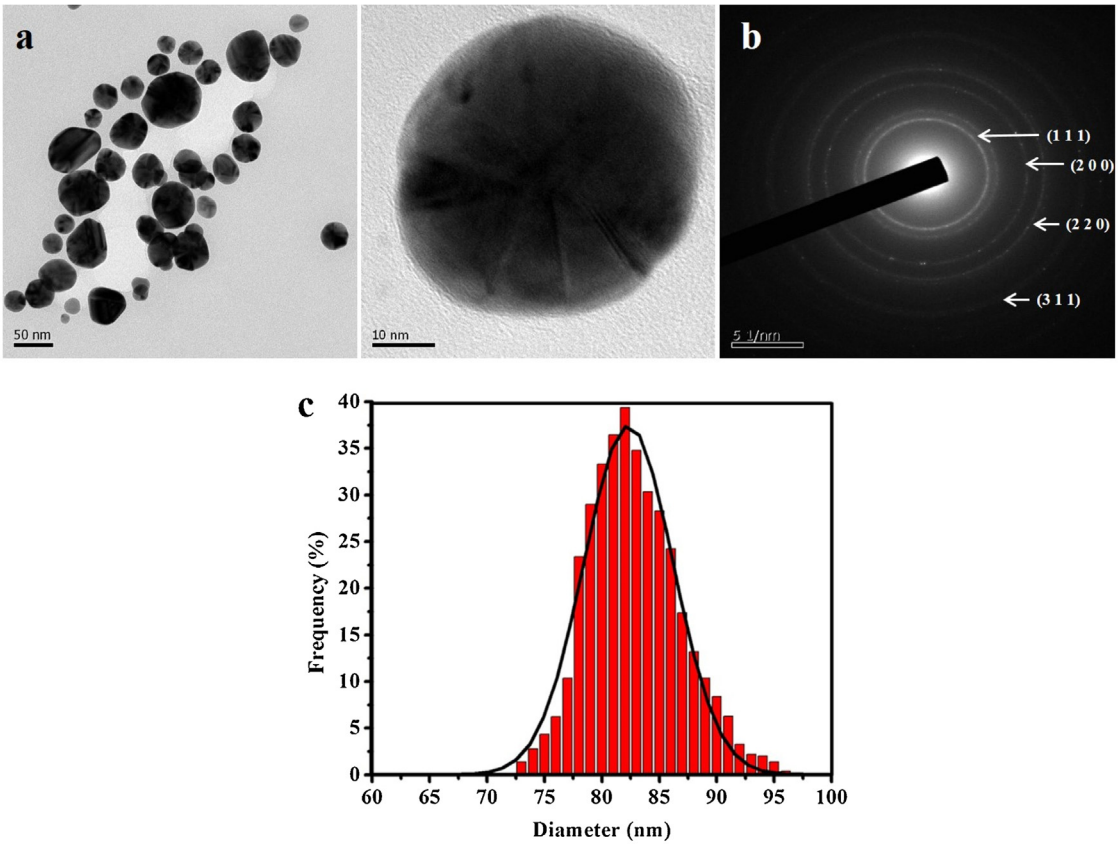

Fig. 2. (a) HRTEM images of fucoidan capped gold nanoparticles. (b) SAED of fucoidan capped gold nanoparticles. (c) DLS histogram of fucoidan capped gold nanoparticles.

with 4% formalin for 10 min. Cells were washed with 1 × PBS and centrifuged at 1500 rpm for 3 min and used for the PAI.

2.7.2. Tissue-mimicking polyvinyl alcohol phantom

Polyvinyl alcohol (PVA) phantoms for imaging were constructed using 8% polyvinyl alcohol (Sigma–Aldrich, St. Louis, USA), 0.4% silica (Min-U-Sil, U.S silica, Pacific, MO, USA) and 100 mL of distilled water. Untreated cells and DOX-Fu AuNPs labeled MDA-MB-231 cells were included in the tissue-mimicking PVA phantom [30]. Untreated cells and DOX-Fu AuNPs labeled MDA-MB-231 cells were mixed with 10% gelatin and used for three inclusions (60 μL each/well) in the tissue-mimicking PVA phantom. Using a micropipette, untreated cells and two different concentrations of DOX-Fu AuNPs labeled MDA-MB-231 cells were poured into each well on PVA phantoms. The gelatin solution was used to cover inclusions after solidification. The PVA phantom was placed in the water tank of the PAI system to obtain images.

2.8. Statistical analysis

Experiments for each sample were performed three times, and final values were presented as the mean ± standard deviation (SD). The statistical software, SPSS/14 (one way ANOVA), was used to estimate statistical parameters. Data obtained were analyzed using Origin Pro 9.0 SRO software (OriginLab Corporation, USA).

3. Results and discussion

In the present study, fucoidan was used as a reducing as well as a stabilizing agent for green synthesis of AuNPs. Furthermore, we have studied that these biosynthesized AuNPs would enable the attachment of biomolecules for drug delivery and PAI (Scheme 1).

3.1. Synthesis and characterization of fu AuNPs

UV–visible spectroscopy is an important technique to determine the formation and stability of AuNPs in aqueous solution. Fucoidan was mixed with chloroauric acid; the mixture turned into a ruby red color within 30 min, which indicated the reduction of Au^{3+} into Au^0 ions, and thus the formation of AuNPs was preliminarily confirmed (Fig. 1a). AuNPs are known to exhibit a ruby red color in aqueous solutions because of the excitation of the surface plasmon resonance (SPR). Biosynthesized AuNPs exhibited a strong peak at 566 nm, which strongly suggests that the AuNPs were spherical in shape.

FTIR spectroscopy is helpful to analyze possible interactions of fucoidan and Fu AuNPs with different functional groups. FTIR spectrum shows the presence of different functional groups at various positions (Fig. 1b). The strong broadband observed at 3444 cm^{-1} and 3441 cm^{-1} in the spectra of fucoidan and Fu AuNPs corresponds to the O—H stretching of alcohols. The band observed at 2933 cm^{-1} and 2932 cm^{-1} were assigned to the C—H stretching of alkanes. The band at 1633 cm^{-1} and 1637 cm^{-1} corresponds to the N—H bending of amines. The medium band at 1256 cm^{-1} and 1260 cm^{-1} can be assigned to the C—H wag of alkyl halides. The band at 1033 cm^{-1} and 1059 cm^{-1} corresponds to the C—N stretching of aliphatic amines.

The XRD technique was used to determine and confirm the crystal structure of nanoparticles. Fig. 1c showed the XRD pattern of dried Fu AuNPs. The intense diffraction peaks were observed at 2θ values of 38.13°, 44.43°, 64.66°, and 77.66°, which correspond to the (111), (200), (220), and (311) reflection of the crystalline metallic gold, respectively (JCPDS no. 04-0784). The well-resolved and intense XRD pattern clearly showed that Fu AuNPs formed by the reduction of Au^{3+} ions using fucoidan are crystalline in nature. Manivasagan et al. reported that the XRD pattern of

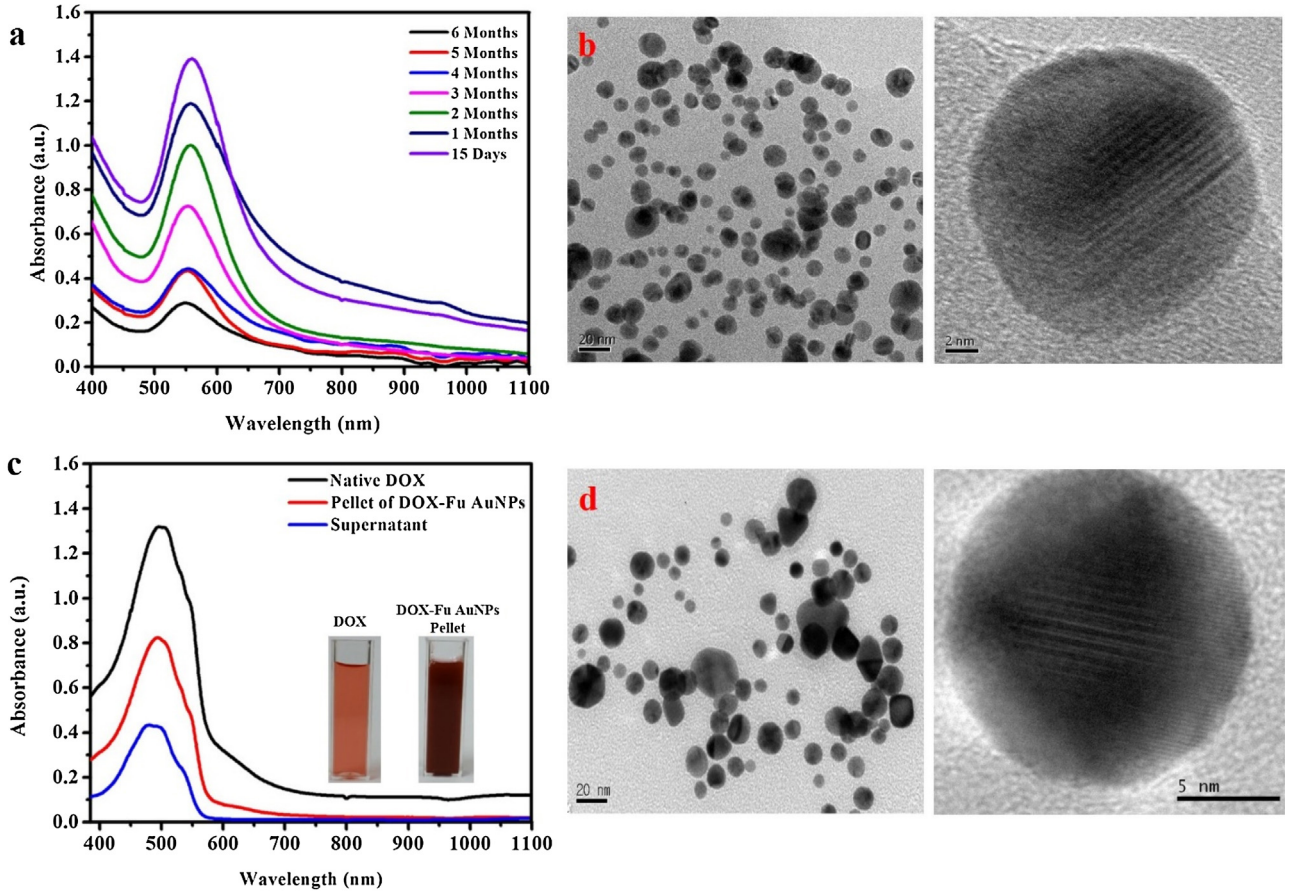

Fig. 3. (a) UV-vis spectral analysis of fucoidan capped gold nanoparticles of six months stability. (b) HRTEM image of fucoidan capped gold nanoparticles of six months stability. (c) UV-vis spectral analysis of native DOX solution, redispersed pellet of DOX-loaded fucoidan capped gold nanoparticles and supernatant of DOX-loaded fucoidan capped gold nanoparticles. (d) HRTEM images of DOX-loaded fucoidan capped gold nanoparticles.

biosynthesized AuNPs corresponded to (111), (200), (220), and (311) of cubic crystalline metallic gold [31].

The morphology of Fu AuNPs as observed by FESEM was well aggregated and spherical in shape. The presence of gold as the major constituent was confirmed by EDX analysis (Fig. 1d). A strong signal for gold at the spectrum of 2.2 keV was characteristic of Fu AuNPs. Interaction with Cu may emerge because of the grid used for analysis, and oxygen peaks may occur because of the biomolecule bound to the surface of Fu AuNPs [32]. Previously, Balasubramani et al. obtained the formation of individual spherical shaped AuNPs in the range 2–2.5 keV in *Chloroxylon swietenia* [33].

HRTEM results gave a clear indication on size and shape of Fu AuNPs (Fig. 2a). Nanoparticles were monodispersed and spherical shaped with size ranging from 73 to 96 nm having an average particle size of ~82 nm. The selected area electron diffraction pattern (SAED) revealed four rings of Brag's reflections corresponding to its face centered cubic nature of Fu AuNPs were find crystalline [34]. Fig. 2b showed that most nanoparticles are nearly spherical in shape with size and the crystalline nature of Fu AuNPs based on SAED pattern. Particle size distribution of Fu AuNPs was analyzed based on measuring the time dependent fluctuation of scattering of light by nanoparticles undergoing Brownian movement [35]. The DLS analysis is used to measure the shell thickness of a capping or stabilizing agent enveloping the metallic nanoparticles along with the actual size of the metallic core. Fig. 2c shows the particle size distribution of Fu AuNPs by means of DLS. The average particle size of the Fu Au NPs was found to be approximately 82 nm. ZP values reveal information regarding the surface charge and stability of biosynthesized Fu AuNPs. ZP measured for Fu AuNPs in the present study was −10.72 mV. ZP analysis indicated that capping molecules present on the surface of AuNPs are mainly comprised of negatively charged groups and also responsible for the moderate stability of nanoparticles. Thus, fucoidan acts as a reducing as well as a capping agent.

For varied biomedical and therapeutic applications, we performed the stability study of Fu AuNPs by monitoring the SPR and HRTEM over 6 months (Fig. 3a and b). The stability of nanoparticles has no shift in SPR and showed no aggregation, indicating that nanoparticles formed were stable. Thus, the long-term stability of nanoparticles could be attributed to electrostatic and mechanical barrier properties of fucoidan. These results laid out the utility of these nanoparticles for drug delivery and PAI.

3.2. Formation of DOX-loaded fucoidan capped gold nanoparticles

After the successful biosynthesis of stable Fu AuNPs, we have visualized this system for drug delivery application through the subsequent loading of a biologically active molecule. Using a delivery system with the non-covalently loaded drug is considered a more rational approach that avoids any potential issues associated with a prodrug strategy. We have selected the anticancer drug DOX for loading on biosynthesized Fu AuNPs. Percent loading of DOX onto Fu AuNPs was determined based on DOX content in the supernatant and obtained pellet, and it was found to be 7.97 ± 2.3% and 92.03 ± 1.5% of DOX, respectively (Fig. 3c). In the HRTEM image, spherical DOX-Fu AuNPs were observed (Fig. 3d). The hydrodynamic particle size of DOX-Fu AuNPs was 83 nm as measured by

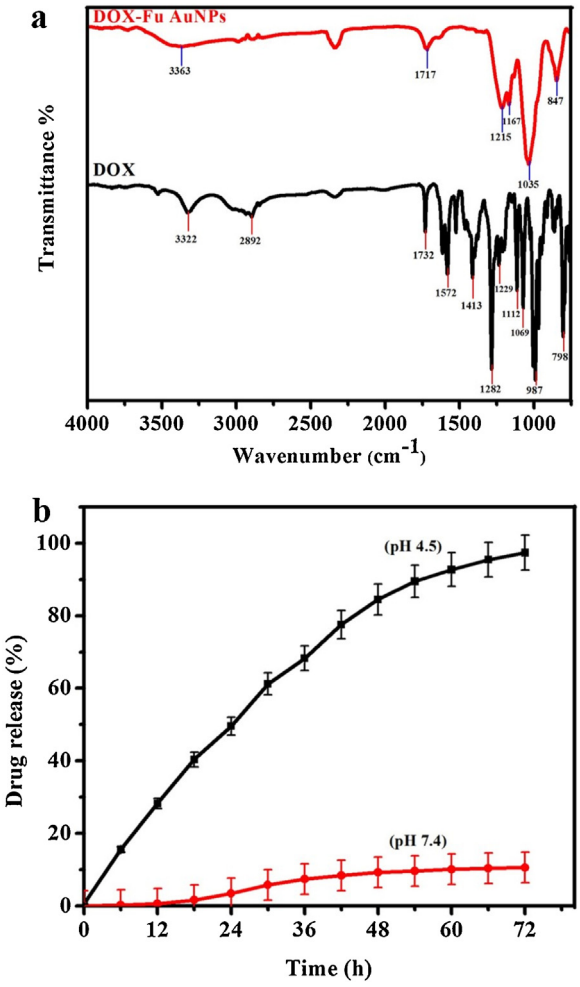

Fig. 4. (a) FTIR spectra of native DOX and DOX-loaded fucoidan capped gold nanoparticles. (b) The drug release profile of DOX from DOX-loaded fucoidan capped gold nanoparticles in acetate buffer and phosphate buffer.

DLS. ZP of DOX-Fu AuNPs was found to be −10.93 mV. ZP of DOX-Fu AuNPs was ascribed to the presence of positively charged DOX on the surface of AuNPs. It was believed that along with the electrostatic interaction other attractive forces, including hydrogen bond could be playing an important role facilitating the drug loading process. The hydrogen bonding between protonated amine groups, evidenced by FTIR (Fig. 4a), where the N—H stretching band at 3322 cm^{-1} of native DOX, shifted to 3363 cm^{-1} in case of DOX-Fu AuNPs. The band observed at 1732 cm^{-1} is assigned to the C=O stretching of aldehydes group whereas the band at 1717 cm^{-1} corresponds to the C=O stretching of unsaturated esters. The band at 1229 cm^{-1} and 1215 cm^{-1} corresponds to the C—H wag of alkyl halides. The medium band observed at 1112 cm^{-1} and 1167 cm^{-1} were assigned to the C—N stretching of aliphatic amines. The band at 1069 cm^{-1} and 1035 cm^{-1} corresponds to the C—N stretching of aliphatic amines.

3.3. Drug release

The ability of the carrier to efficiently release the cargo at the desired site is an important feature of any delivery system. Fig. 4b represents the release of DOX from DOX-Fu AuNPs in acetate buffer (pH 4.5) and phosphate buffer (pH 7.4). At the end of 72 h, 97% and 10% of DOX was released in acetate and phosphate buffer, respectively. This revealed that the release of DOX was greater in acidic pH than in neutral pH. This pH-dependent release may help improve the efficiency of DOX as the uptake of drug-loaded nanoparticle through endocytosis process leads to exposure to an acidic environment [36]. This may initiate rapid release of DOX from DOX-Fu AuNPs after internalization. Such efficient release would ultimately result in improved cytotoxic activity against cancer cells. Furthermore, the negligible release of DOX from DOX-Fu AuNPs in neutral pH will help reduce the toxicity of DOX to the normal tissue as the physiological pH of the body is maintained at pH 7.4 [37]. Prabaharan et al. [38] investigated the gold nanoparticles stabilized with a monolayer of doxorubicin-conjugated amphiphilic block copolymer for tumor-targeted drug delivery. The conjugated DOX was released from the folate (FA)-conjugated amphiphilic Au NPs with a poly(L-aspartate-doxorubicin)-b-poly(ethylene glycol) monolayer (Au-P(LA-DOX)-b-PEG-OH/FA) micelles much more rapidly at pH 5.3 and 6.6 that at pH 7.4, which is a desirable characteristics for tumor-targeted drug delivery. Banu et al. [39] reported that doxorubicin loaded polymeric gold nanoparticles evaluated in an acidic pH to analyze the *in vitro* drug release of the drug delivery system. Wang et al. [40] developed the doxorubicin-tethered responsive gold nanoparticles (DOX-Hyd@AuNPs) facilitate intracellular drug delivery for overcoming multidrug resistance in cancer cells. The release of DOX was higher in acidic pH 5.0 as compared to neutral pH 7.4. You et al. [41] reported the doxorubicin loaded hollow gold nanospheres for anticancer therapy. The release of DOX was also pH-dependent, with more DOX released in aqueous solution at lower pH.

3.4. In vitro *cytotoxic activity*

AuNPs as novel agents for cancer therapy are gaining greater demand in medical applications. At the same time, there are only limited studies on the cytotoxic effect of green synthesized AuNPs against cancer cell lines [31]. This is the first study to report DOX-Fu AuNPs against MDA-MB-231 cells. In the present study, the *in vitro* cytotoxic effects of fucoidan, Fu AuNPs, DOX, and DOX-Fu AuNPs were evaluated against MDA-MB-231 cells at different concentrations (Fig. 5a). They showed a dose-dependent decrease in cell viability. Fifty percentage of cell death, which determines the IC_{50} value of fucoidan, Fu AuNPs, DOX, and DOX-Fu AuNPs against MDA-MB-231 cells, holds at 35 μg/mL, 30 μg/mL, 15 μg/mL, and 5 μg/mL in 24 h. The experimental results clearly proved the excellent anticancer activity of DOX-Fu AuNPs against MDA-MB-231 cells. Previously, Venkatpurwar et al. reported the porphyran capped AuNPs as novel carriers for anticancer drug delivery. DOX-loaded AuNPs demonstrated higher cytotoxicity on LN-229 cell line than did an equal dose of native DOX solution [11]. Lee et al. [4] reported the doxorubicin loading fucoidan acetate nanoparticles (DOX-AcFu) for immune- and chemotherapy in cancer treatment. IC_{50} value of DOX-AcFu was lower than that of free DOX in the multidrug resistance model cells.

3.5. *Induction of apoptosis by DOX-Fu AuNPs*

3.5.1. *Morphological observation*

Morphological changes were observed in DOX-Fu AuNPs-treated MDA-MB-231 cells when compared with untreated cells. The most recognizable morphological changes of DOX-Fu AuNPs-treated cells observed in this study was membrane integrity loss, cell growth inhibition, cytoplasmic condensation, and cell clumping (Fig. 5b).

3.5.2. *Propidium iodide staining*

PI reacts with both DNA and RNA and is a commonly used fluorescent reagent for nucleic acid staining. The induction of apoptosis, after treatment with IC_{50} concentration of DOX-Fu AuNPs, was assessed by fluorescence microscopy after staining with PI, and

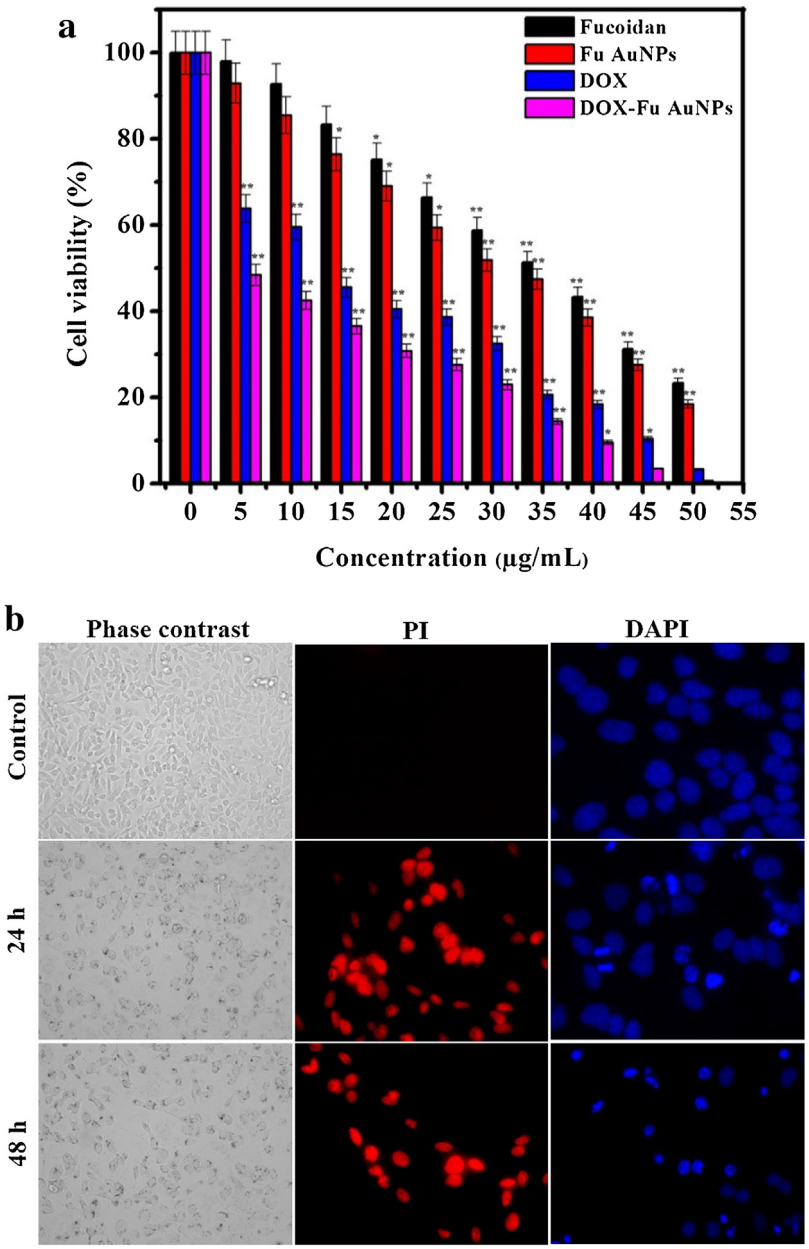

Fig. 5. (a) MTT assay results confirming the *in vitro* cytotoxicity effect of fucoidan, fucoidan capped gold nanoparticles, native DOX, and DOX-loaded fucoidan capped gold nanoparticles against MDA-MB-231 cells for 24 h. Data is expressed as mean ± SD of the three experiments. Percentage of cytotoxicity is expressed relative to untreated controls (*significant $p < 0.05$; **highly significant $p < 0.01$). (b) Morphological alterations in MDA-MB-231 cells incubated with 5 μg/mL of DOX-loaded fucoidan capped gold nanoparticles for 24 and 48 h, as assessed by contrast phase microcopy (20 × Magnification). Propidium iodide staining of MDA-MB-231 cells in control and treated with 5 μg/mL of DOX-loaded fucoidan capped gold nanoparticles for 24 and 48 h (40 × Magnification). DAPI nuclear staining of control cells and DOX-loaded fucoidan capped gold nanoparticles treated cells exhibited condensed form of nuclear materials in apoptotic cells.

it showed apoptotic changes and nuclear condensation. In case of control cells, a negligible number of PI-positive cells were noticed. In contrast, progressive increase in the number of PI-positive cells was noted in DOX-Fu AuNPs-treated cells (Fig. 5b). These data suggest that DOX-Fu AuNPs can induce cell death in MDA-MB-231 cells through the reactive oxygen species (ROS)-mediated apoptotic process. Increased ROS levels and subsequent loss of mitochondria membrane potential may be the reason for increased apoptotic morphological changes in DOX-Fu AuNPs-treated cells [42].

3.5.3. 4′,6-diamidino-2-phenylindole dihydrochloride staining

DAPI is a fluorescent stain mainly used to detect different characteristic features of apoptotic process. In DAPI staining, after treatment with IC_{50} concentration of DOX-Fu AuNPs for 24 and 48 h, MDA-MB-231 cells start to exhibit apoptotic characteristics, such as cell shrinkage, nuclear condensation, and fragmentation. In the control group, cells were regular in morphology and showed an intact nuclear structure (Fig. 5b). Interestingly, some studies have reported that AuNps can also induce DNA damage and apoptosis in cancer cells [31].

3.5.4. Flow cytometry analysis

Annexin V/PI double staining was used to detect apoptosis in MDA-MB-231 cells. Fig. 6a shows the degree of apoptosis caused by the DOX-Fu AuNPs delivery system as assessed by the FACS analysis. MDA-MB-231 cells were treated with an IC_{50} concentration of DOX-Fu AuNPs for 24 and 48 h. DOX-Fu AuNPs induced both early and late apoptosis in a concentration-dependent manner compared

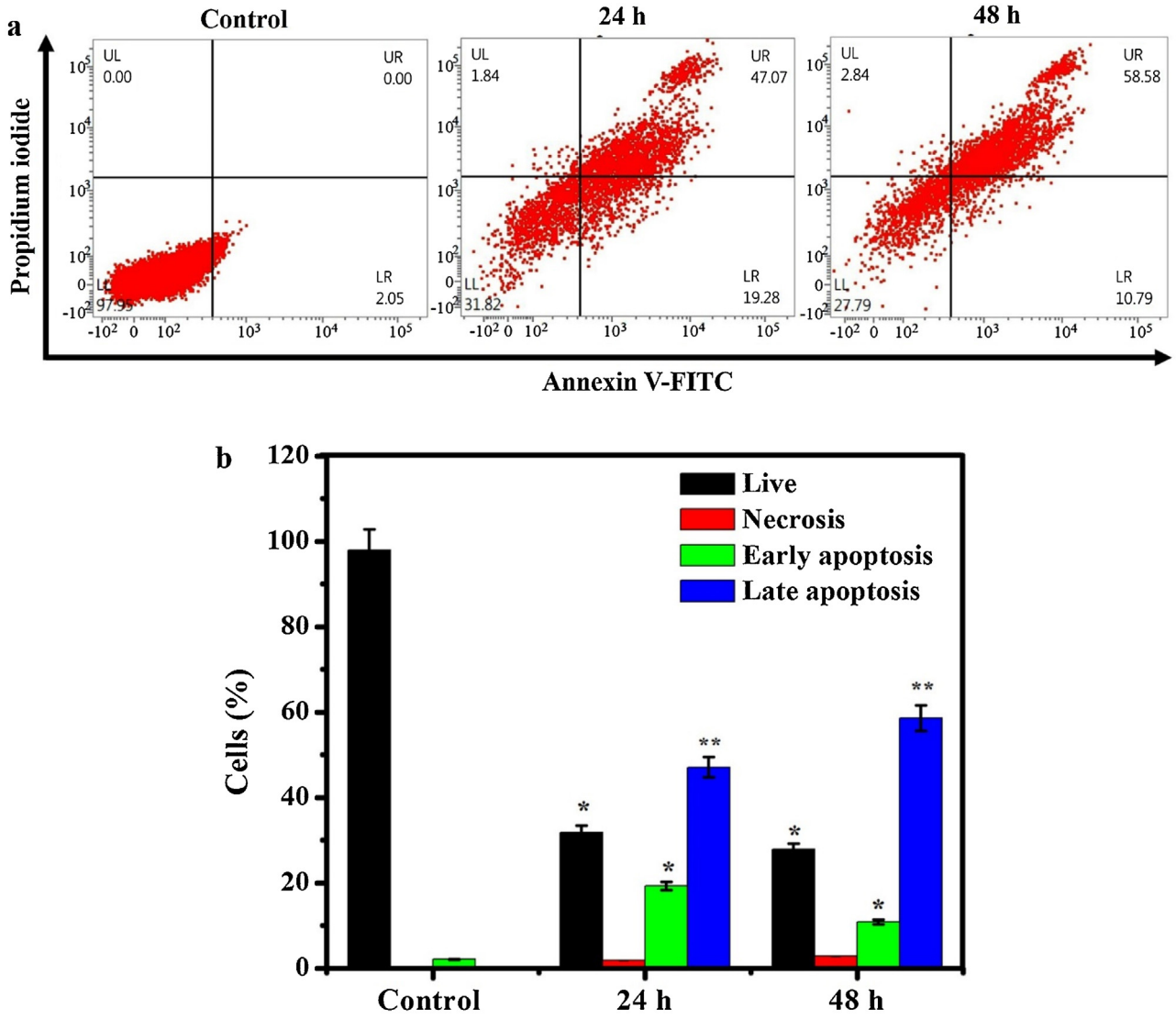

Fig. 6. (a) Fluorescence-activated cell sorting (FACS) analysis of apoptosis in MDA-MB-231 cells incubated with 5 μg/mL of DOX-loaded fucoidan capped gold nanoparticles measured using fluorescein isothiocyanate (FITC)-labeled Annexin V and PI. Representative dot plots showing the distribution of Annexin V and PI staining for control and DOX-Fu AuNPs-treated cells. (b) Bar graph represents the mean percentages of apoptosis and necrosis (*significant $p < 0.05$; ** highly significant $p < 0.01$).

with untreated control cells. When cells were treated with IC_{50} concentration of DOX-Fu AuNPs for 24 and 48 h, the average proportion of Annexin V-staining positive cells (total apoptotic cells) significantly increased from 2.05% in control to 66.35% and 69.37% respectively (Fig. 6b).

3.6. Photoacoustic imaging

Fig. 7b shows the top view of the tissue-mimicking PVA phantom including three inclusions of untreated cells (control) and two different concentrations of DOX-Fu AuNPs-labeled MDA-MB-231 cells (5 and 10 μg/mL). The maximum intensity projection (MIP) image along the *z*-axis to *xy* plane of the phantom (Fig. 7c) is displayed over a 26 mm × 7 mm field of view. It clearly reveals the distribution of DOX-Fu AuNPs labeled MDA-MB-231 cells inside the phantom. The high-amplitude photoacoustic signals could not be detected in untreated cells (control), which were not DOX-Fu AuNPs. The high-amplitude photoacoustic signals were detected from inclusions of high concentration of DOX-Fu AuNPs-labeled MDA-MB-231 cells (10 μg/mL). The incident light homogeneously distributed over the volume of inclusions containing DOX-Fu AuNPs-labeled MDA-MB-231 cells because of the optical scattering inside the cells. Fig. 7d shows the three dimensional photoacoustic image of the phantom with the 26 mm × 7 mm × 6 mm field of view. Biological targeting of DOX-Fu AuNPs to cancer cells may further increase the magnitude or change the pattern of DOX-Fu AuNPs accumulation inside cancer cells. This could be well studied using PAI as demonstrated here. The ability to image DOX-Fu AuNPs inside cancer cells with PAI also suggests an opportunity for image-guided cancer therapy, with DOX-Fu AuNPs serving as cancer imaging contrast agents and mediators of cancer therapy. The presently employed laser system (532 nm) for PAT, used in conjunction with DOX-Fu AuNPs as a contrast agent, has the potential to allow for non-invasive early diagnosis and image-guided treatment of superficial, often refractory, tumors such as breast cancer, malignant melanoma, and Merkel cell carcinoma.

4. Conclusion

Nanobiotechnology represents a new era of an innovative approach to develop and test modern drug formulations based on biosynthesized nanoparticles for drug delivery and PAI. In the

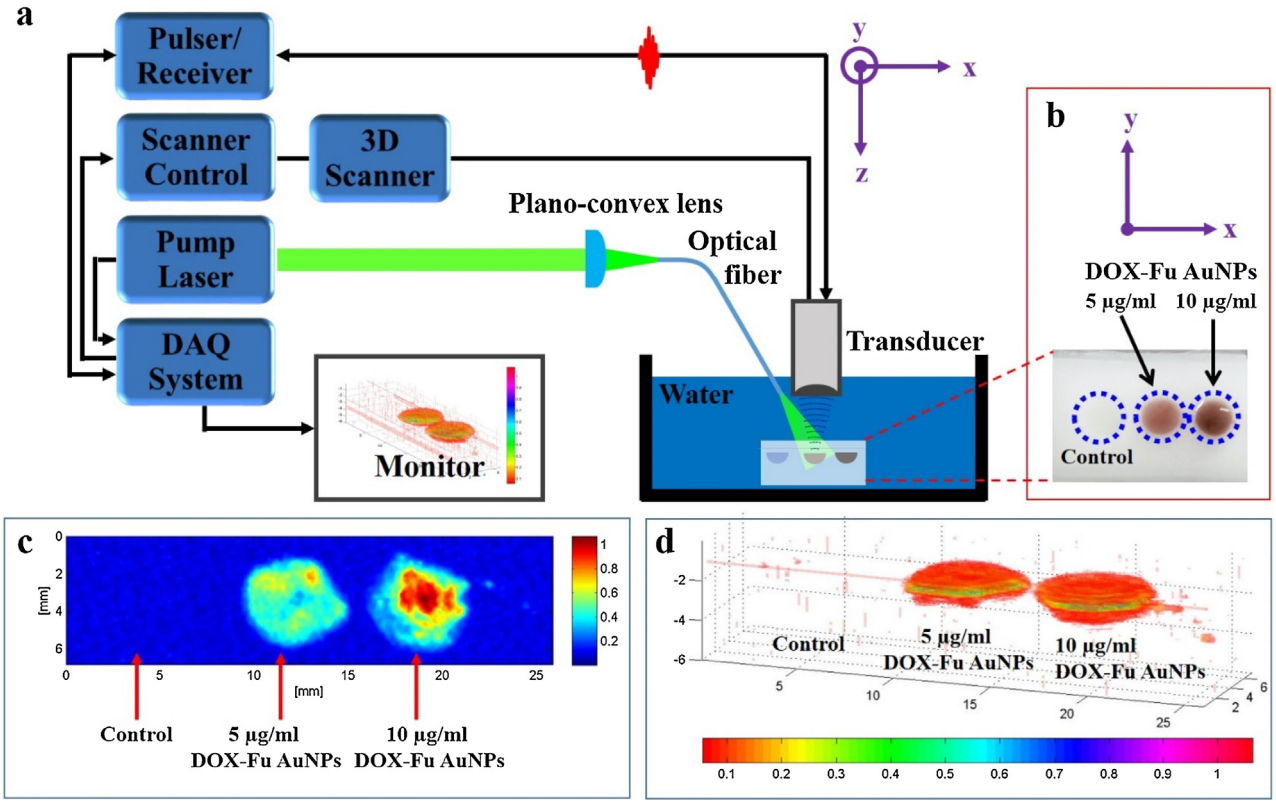

Fig. 7. (a) Diagram of the photoacoustic imaging system used to image the tissue mimicking PVA phantom. (b) Diagram of tissue mimicking polyvinyl alcohol phantom shows a top view structure. (c) Photoacoustic image of untreated cells (control) and two different concentrations of DOX-Fu AuNPs labeled MDA-MB-231 cells (5 and 10 μg/mL). (d) Three dimensional (3D) photoacoustic image of untreated cells (control) and two different concentrations of DOX-Fu AuNPs labeled MDA-MB-231 cells (5 and 10 μg/mL).

present study, we have demonstrated a novel method for the green synthesis of AuNPs using a biocompatible polymer, fucoidan with improved surface properties for binding of biomolecules. Synthesized AuNPs were characterized using spectroscopic and microscopic techniques. Further, the applicability of these nanoparticles as a carrier for the delivery of cationic anticancer drugs was demonstrated by successful loading of DOX onto synthesized AuNPs. This is the first report on the multifunctional DOX-Fu AuNPs for drug delivery and PAI. The *in vitro* cytotoxicity of DOX-Fu AuNPs can be attributed to the greater uptake potential of Fu AuNPs, thus establishing the role of AuNPs as efficient carriers for the delivery of anticancer drugs. These DOX-Fu AuNPs showed a *p*H-dependent release behavior with the negligible release of DOX in basic *p*H, which may help to reduce the toxicity of DOX to the normal tissue. The flow cytometry techniques represent very useful tools for a variety of biological and clinical studies requiring quantitative information regarding cell death; apoptosis analysis was performed through Annexin V-FITC/PI dual staining and cellular DNA content analysis. DOX-Fu AuNPs have been used as a contrast agent for imaging with PAI *in vitro* and for noninvasive detection in MDA-MB-231 cells. The ability to image DOX-Fu AuNPs has important implications for developing these biocompatible nanoparticles for cancer diagnostic and therapeutic application. In the light of these results, DOX-Fu AuNPs could be considered as a promising candidate for drug delivery and PAI. Therefore, we hope that these multifunctional DOX-Fu AuNPs for drug delivery and PAI can soon provide great contributions to human health.

Acknowledgement

This work was supported by a research grant of Pukyong National University in 2014.

References

[1] P. Manivasagan, J. Oh, Marine polysaccharide-based nanomaterials as a novel source of nanobiotechnological applications, Int. J. Biol. Macromol. 82 (2016) 315–327.
[2] M. Lira, N. Santos-Magalhães, V. Nicolas, V. Marsaud, M. Silva, G. Ponchel, C. Vauthier, Cytotoxicity and cellular uptake of newly synthesized fucoidan-coated nanoparticles, Eur. J. Pharm. Biopharm. 79 (1) (2011) 162–170.
[3] M.E. Duarte, M.A. Cardoso, M.D. Noseda, A.S. Cerezo, Structural studies on fucoidans from the brown seaweed *Sargassum stenophyllum*, Carbohydr. Res. 333 (4) (2001) 281–293.
[4] K.W. Lee, D. Jeong, K. Na, Doxorubicin loading fucoidan acetate nanoparticles for immune and chemotherapy in cancer treatment, Carbohydr. Res. 94 (2) (2013) 850–856.
[5] M. Kusaykin, I. Bakunina, V. Sova, S. Ermakova, T. Kuznetsova, N. Besednova, T. Zaporozhets, T. Zvyagintseva, Structure, biological activity, and enzymatic transformation of fucoidans from the brown seaweeds, Biotechnol. J. 3 (7) (2008) 904–915.
[6] J. Ma, Y. Zou, Z. Jiang, W. Huang, J. Li, G. Wu, Y. Huang, H. Xu, An in situ XAFS study—the formation mechanism of gold nanoparticles from X-ray-irradiated ionic liquid, Phys. Chem. Chem. Phys. 15 (28) (2013) 11904–11908.
[7] S. Mukherjee, S. Sau, D. Madhuri, V.S. Bollu, K. Madhusudana, B. Sreedhar, R. Banerjee, C.R. Patra, Green synthesis and characterization of monodispersed gold nanoparticles: toxicity study, delivery of doxorubicin and its bio-distribution in mouse model, J. Biomed. Nanotechnol. 12 (1) (2016) 165–181.
[8] P. Manivasagan, J. Venkatesan, K.-H. Kang, K. Sivakumar, S.-J. Park, S.-K. Kim, Production of α-amylase for the biosynthesis of gold nanoparticles using *Streptomyces* sp. MBRC-82, Int. J. Biol. Macromol. 72 (2015) 71–78.
[9] J. Kimling, M. Maier, B. Okenve, V. Kotaidis, H. Ballot, A. Plech, Turkevich method for gold nanoparticle synthesis revisited, J. Phys. Chem. B 110 (32) (2006) 15700–15707.
[10] D.R. Bhumkar, H.M. Joshi, M. Sastry, V.B. Pokharkar, Chitosan reduced gold nanoparticles as novel carriers for transmucosal delivery of insulin, Pharm. Res. 24 (8) (2007) 1415–1426.
[11] V. Venkatpurwar, A. Shiras, V. Pokharkar, Porphyran capped gold nanoparticles as a novel carrier for delivery of anticancer drug: *in vitro* cytotoxicity study, Int. J. Pharm. 409 (1) (2011) 314–320.

[12] B. Asadishad, M. Vossoughi, I. Alamzadeh, *In vitro* release behavior and cytotoxicity of doxorubicin-loaded gold nanoparticles in cancerous cells, Biotechnol. Rep. 32 (5) (2010) 649–654.
[13] J. Zhang, S. Rana, R. Srivastava, R. Misra, On the chemical synthesis and drug delivery response of folate receptor-activated, polyethylene glycol-functionalized magnetite nanoparticles, Acta Biomater. 4 (1) (2008) 40–48.
[14] W. Lu, Q. Sun, J. Wan, Z. She, X.-G. Jiang, Cationic albumin–conjugated pegylated nanoparticles allow gene delivery into brain tumors via intravenous administration, Cancer Res. 66 (24) (2006) 11878–11887.
[15] C. Krishnaraj, P. Muthukumaran, R. Ramachandran, M. Balakumaran, P. Kalaichelvan, Acalypha indica Linn: biogenic synthesis of silver and gold nanoparticles and their cytotoxic effects against MDA-MB-231 human breast cancer cells, Biotechnol. Rep. 4 (2014) 42–49.
[16] T.-c. Hsieh, E.K. Wijeratne, J.-y. Liang, A.L. Gunatilaka, J.M. Wu, Differential control of growth, cell cycle progression, and expression of NF-κB in human breast cancer cells MCF-7, MCF-10A, and MDA-MB-231 by ponicidin and oridonin, diterpenoids from the chinese herb *Rabdosia rubescens*, Biochem. Biophys. Res. Commun. 337 (1) (2005) 224–231.
[17] L. Yeruva, J.A. Elegbede, S.W. Carper, Methyl jasmonate decreases membrane fluidity and induces apoptosis via tumor necrosis factor receptor 1 in breast cancer cells, Anticancer Drugs 19 (8) (2008) 766–776.
[18] J. Fong, F. Wood, Nanocrystalline silver dressings in wound management: a review, Int. J. Nanomed. 1 (4) (2006) 441–449.
[19] W. Lu, Q. Huang, G. Ku, X. Wen, M. Zhou, D. Guzatov, P. Brecht, R. Su, A. Oraevsky, L.V. Wang, Photoacoustic imaging of living mouse brain vasculature using hollow gold nanospheres, Biomaterials 31 (9) (2010) 2617–2626.
[20] R.O. Esenaliev, I.V. Larina, K.V. Larin, D.J. Deyo, M. Motamedi, D.S. Prough, Optoacoustic technique for noninvasive monitoring of blood oxygenation: a feasibility study, Appl. Optics 41 (22) (2002) 4722–4731.
[21] C.-W. Wei, S.-W. Huang, C.-R.C. Wang, P.-C. Li, Photoacoustic flow measurements based on wash-in analysis of gold nanorods, Ultrason. Ferroelectr. Freq. Control IEEE Trans. 54 (6) (2007) 1131–1141.
[22] P.-C. Li, C.-R.C. Wang, D.-B. Shieh, C.-W. Wei, C.-K. Liao, C. Poe, S. Jhan, A.-A. Ding, Y.-N. Wu, In vivo photoacoustic molecular imaging with simultaneous multiple selective targeting using antibody-conjugated gold nanorods, Opt. Express 16 (23) (2008) 18605–18615.
[23] P. Sharma, S.C. Brown, N. Bengtsson, Q. Zhang, G.A. Walter, S.R. Grobmyer, S. Santra, H. Jiang, E.W. Scott, B.M. Moudgil, Gold-speckled multimodal nanoparticles for noninvasive bioimaging, Chem. Mater. 20 (19) (2008) 6087–6094.
[24] R.M. Rodriguez-Jasso, S.I. Mussatto, L. Pastrana, C.N. Aguilar, J.A. Teixeira, Microwave-assisted extraction of sulfated polysaccharides (fucoidan) from brown seaweed, Carbohydr. Polym. 86 (3) (2011) 1137–1144.
[25] A. Synytsya, W.-J. Kim, S.-M. Kim, R. Pohl, A. Synytsya, F. Kvasnička, J. Čopíková, Y.I. Park, Structure and antitumour activity of fucoidan isolated from sporophyll of Korean brown seaweed *Undaria pinnatifida*, Carbohydr. Polym. 81 (1) (2010) 41–48.
[26] A.D. Holtkamp, S. Kelly, R. Ulber, S. Lang, Fucoidans and fucoidanases—focus on techniques for molecular structure elucidation and modification of marine polysaccharides, Appl. Microbiol. Biotechnol. 82 (1) (2009) 1–11.
[27] D. Prabhu, C. Arulvasu, G. Babu, R. Manikandan, P. Srinivasan, Biologically synthesized green silver nanoparticles from leaf extract of *Vitex negundo* L. induce growth-inhibitory effect on human colon cancer cell line HCT15, Process Biochem. 48 (2) (2013) 317–324.
[28] P. Manivasagan, M.S. Alam, K.-H. Kang, M. Kwak, S.-K. Kim, Extracellular synthesis of gold bionanoparticles by *Nocardiopsis* sp. and evaluation of its antimicrobial, antioxidant and cytotoxic activities, Bioprocress Biosyst. Eng. 38 (6) (2015) 1167–1177.
[29] I. Bhatnagar, J. Venkatesan, S.-K. Kim, Polymer functionalized single walled carbon nanotubes mediated drug delivery of gliotoxin in cancer cells, J. Biomed. Nanotechnol. 10 (1) (2014) 120–130.
[30] N.Q. Bui, K.K. Hlaing, V.P. Nguyen, T.H. Nguyen, Y.-O. Oh, X.F. Fan, Y.W. Lee, S.Y. Nam, H.W. Kang, J. Oh, Intravascular ultrasonic–photoacoustic (IVUP) endoscope with 2.2-mm diameter catheter for medical imaging, Comput. Med. Imaging Grapics 45 (2015) 57–62.
[31] P. Manivasagan, J. Oh, Production of a novel fucoidanase for the green synthesis of gold nanoparticles by *Streptomyces* sp. and its cytotoxic effect on HeLa cells, Mar. Drugs 13 (11) (2015) 6818–6837.
[32] Y. Wang, X. He, K. Wang, X. Zhang, W. Tan, *Barbated Skullcup* herb extract-mediated biosynthesis of gold nanoparticles and its primary application in electrochemistry, Colloids Surf. B 73 (1) (2009) 75–79.
[33] G. Balasubramani, R. Ramkumar, N. Krishnaveni, R. Sowmiya, P. Deepak, D. Arul, P. Perumal, GC–MS analysis of bioactive components and synthesis of gold nanoparticle using *Chloroxylon swietenia* DC leaf extract and its larvicidal activity, J. Photochem. Photobiol. B 148 (2015) 1–8.
[34] P. Karuppaiya, E. Satheeshkumar, W.-T. Chao, L.-Y. Kao, E.C.-F. Chen, H.-S. Tsay, Anti-metastatic activity of biologically synthesized gold nanoparticles on human fibrosarcoma cell line HT-1080, Colloids Surf. B 110 (2013) 163–170.
[35] F.A.A. Rajathi, C. Parthiban, V.G. Kumar, P. Anantharaman, Biosynthesis of antibacterial gold nanoparticles using brown alga, *Stoechospermum marginatum* (kützing), Spectrochim. Acta 99 (2012) 166–173.
[36] L.M. Bareford, P.W. Swaan, Endocytic mechanisms for targeted drug delivery, Adv. Drug Delivery Rev. 59 (8) (2007) 748–758.
[37] S. Aryal, J.J. Grailer, S. Pilla, D.A. Steeber, S. Gong, Doxorubicin conjugated gold nanoparticles as water-soluble and pH-responsive anticancer drug nanocarriers, J. Mater. Chem. 19 (42) (2009) 7879–7884.
[38] M. Prabaharan, J.J. Grailer, S. Pilla, D.A. Steeber, S. Gong, Gold nanoparticles with a monolayer of doxorubicin-conjugated amphiphilic block copolymer for tumor-targeted drug delivery, Biomaterials 30 (30) (2009) 6065–6075.
[39] H. Banu, D.K. Sethi, A. Edgar, A. Sheriff, N. Rayees, N. Renuka, S. Faheem, K. Premkumar, G. Vasanthakumar, Doxorubicin loaded polymeric gold nanoparticles targeted to human folate receptor upon laser photothermal therapy potentiates chemotherapy in breast cancer cell lines, J. Photochem. Photobiol. B 149 (2015) 116–128.
[40] F. Wang, Y.-C. Wang, S. Dou, M.-H. Xiong, T.-M. Sun, J. Wang, Doxorubicin-tethered responsive gold nanoparticles facilitate intracellular drug delivery for overcoming multidrug resistance in cancer cells, ACS Nano 5 (5) (2011) 3679–3692.
[41] J. You, G. Zhang, C. Li, Exceptionally high payload of doxorubicin in hollow gold nanospheres for near-infrared light-triggered drug release, ACS Nano 4 (2) (2010) 1033–1041.
[42] M.J. Piao, K.A. Kang, I.K. Lee, H.S. Kim, S. Kim, J.Y. Choi, J. Choi, J.W. Hyun, Silver nanoparticles induce oxidative cell damage in human liver cells through inhibition of reduced glutathione and induction of mitochondria-involved apoptosis, Toxicol. Lett. 201 (1) (2011) 92–100.